Mechanosensitive channel inhibition attenuates TGFβ2-induced actin cytoskeletal remodeling and reactivity in mouse optic nerve head astrocytes

Alexander Kirschner[a], Ana N. Strat[a,b], John Yablonski[a], Hannah Yoo[a], Tyler Bagué[a], Haiyan Li[a,c,d], Jing Zhao[e,f], Kathryn E. Bollinger[e,f], Samuel Herberg[a,c,d,g,h], Preethi S. Ganapathy[a,b,d,*]

[a]Department of Ophthalmology & Visual Sciences, SUNY Upstate Medical University, Syracuse, NY, 13210, USA

[b]Department of Neuroscience and Physiology, SUNY Upstate Medical University, Syracuse, NY, 13210, USA

[c]Department of Cell and Developmental Biology, SUNY Upstate Medical University, Syracuse, NY, 13210, USA

[d]BioInspired Institute, Syracuse University, Syracuse, NY, 13244, USA

[e]Department of Ophthalmology, Medical College of Georgia at Augusta University, Augusta, GA, 30912, USA

[f]Culver Vision Discovery Institute, Augusta, GA, 30912, USA

[g]Department of Biochemistry and Molecular Biology, SUNY Upstate Medical University, Syracuse, NY, 13210, USA

[h]Department of Biomedical and Chemical Engineering, Syracuse University, Syracuse, NY, 13244, USA

Abstract

Astrocytes within the optic nerve head undergo actin cytoskeletal rearrangement early in glaucoma, which coincides with astrocyte reactivity and extracellular matrix (ECM) deposition. Elevated transforming growth factor beta 2 (TGFβ2) levels within astrocytes have been described in glaucoma, and TGFβ signaling induces actin cytoskeletal remodeling and ECM deposition in many tissues. A key mechanism by which astrocytes sense and respond to external stimuli is via mechanosensitive ion channels. Here, we tested the hypothesis that inhibition of mechanosensitive

channels will attenuate TGFβ2-mediated optic nerve head astrocyte actin cytoskeletal remodeling, reactivity, and ECM deposition. Primary optic nerve head astrocytes were isolated from C57BL/6J mice and cell purity was confirmed by immunostaining. Astrocytes were treated with vehicle control, TGFβ2 (5 ng/ml), GsMTx4 (a mechanosensitive channel inhibitor; 500 nM), or TGFβ2 (5 ng/ml) + GsMTx4 (500 nM) for 48 h. FITC-phalloidin staining was used to assess the formation of f-actin stress fibers and to quantify the presence of crosslinked actin networks (CLANs). Cell reactivity was determined by immunostaining and immunoblotting for GFAP. Levels of fibronectin and collagen IV deposition were also quantified. Primary optic nerve head astrocytes were positive for the astrocyte marker GFAP and negative for markers for microglia (F4/80) and oligodendrocytes (OSP1). Significantly increased %CLAN-positive cells were observed after 48-h treatment with TGFβ2 vs. control in a dose-dependent manner. Co-treatment with GsMTx4 significantly decreased %CLAN-positive cells vs. TGFβ2 treatment and the presence of f-actin stress fibers. TGFβ2 treatment significantly increased GFAP, fibronectin, and collagen IV levels, and GsMTx4 co-treatment ameliorated GFAP immunoreactivity. Our data suggest inhibition of mechanosensitive channel activity as a potential therapeutic strategy to modulate actin cytoskeletal remodeling within the optic nerve head in glaucoma.

Keywords

Transforming growth factor beta 2; Extracellular matrix; Cross-linked actin networks; CLAN; Glaucoma; POAG; Gliosis; Fibronectin

1. Introduction

Glaucoma is a leading cause of irreversible blindness, characterized by retinal ganglion cell death (Quigley and Broman, 2006; Tham et al., 2014). A key site of glaucomatous ganglion cell injury is at the optic nerve head (ONH) (Anderson and Hendrickson, 1974; Quigley and Anderson, 1976; Quigley et al., 1979). Although there are differences in ONH structure across species, the matrix and cellular composition are remarkably consistent (Morrison et al., 1988; Howell et al., 2007; Morrison et al., 2011). This region contains astrocytes, lamina cribrosa cells and microglia in an extracellular matrix (ECM) scaffold that provides structural support to retinal ganglion cell axons as they exit the globe (Hernandez et al., 1987; Hernandez et al., 1988). In glaucoma, the ONH ECM structure undergoes remodeling and stiffening, which correlates with mechanical insult on ganglion cell axons (Crawford Downs, Roberts et al., 2011; Voorhees et al., 2017; Liu et al., 2018; Pijanka et al., 2019; Hopkins et al., 2020). However, the mechanism of this stiffening response remains unclear. One likely modifier of ECM structure is the profibrotic cytokine transforming growth factor beta 2 (TGFβ2). Elevated levels of TGFβ2 have been documented in the glaucomatous ONH, and TGFβ2 directly increases ECM deposition by ONH cells (Pena et al., 1999; Fuchshofer et al., 2005; Zode et al., 2011).

Due to their close interactions with the ECM and retinal ganglion cell axons, ONH astrocytes are the most likely sensors of pathologic stimuli (Hernandez, 2000, May and Lutjen-Drecoll, 2002; Morrison et al., 2011). Thus, they are ideally positioned to sense stressors and transduce this insult into changes in ECM makeup and ganglion cell

axonal health. In response to glaucomatous injury, astrocytes immediately reorganize their cytoskeletal structure and undergo significant process reorientation (Cooper et al., 2018; Tehrani et al., 2019; Cooper et al., 2020). These cytoskeletal changes coincide with the development of astrocyte reactive gliosis, which correlates with cellular hypertrophy and upregulation of glial fibrillary acid protein (GFAP) (Cooper et al., 2018). There is clear evidence that astrocyte mobilization and reactive gliosis are protective to retinal ganglion cells in experimental models of glaucoma (Sun et al., 2017; Cooper et al., 2020). However, it is possible that the later effects of unrestricted astrocyte gliosis ultimately contribute to ONH ECM dysregulation and subsequent ganglion cell insult.

A key mechanism by which cells sense and respond to external stimuli is via mechanosensitive ion channels (Petho et al., 2019). Both Transient Receptor Protein and Piezo channels have been identified in the ONH (Choi et al., 2015). In response to mechanical stimuli, these channels are activated by direct lipid-stretch or via integrin-mediated stimulation to permit calcium influx to effect downstream signaling (Petho et al., 2019). In normal conditions, these channels respond to mechanical cues to guide developmental and physiologic cellular organization. By contrast, in pathologic states, dysregulated astrocyte mechanosensitive channel activity alters the actin network, ultimately promoting mechanosensitive channel expression via a positive feedback loop (Chen et al., 2018). Indeed, Piezo1 stimulation directly induces ONH astrocyte gliosis (Liu et al., 2021); yet, the role of astrocyte mechanosensation in glaucoma is not well understood.

Taken together, TGFβ2 is strongly linked to astrocyte cytoskeletal remodeling and reactive gliosis, and mechanosensitive channel activity can directly regulate actin cytoskeletal reorganization. Thus, modulation of mechanosensitive channels represents an attractive strategy to target astrocyte behavior in glaucoma. In the present study, we tested the hypothesis that inhibition of mechanosensitive channels attenuates TGFβ2-induced actin reorganization, reactive gliosis, and ECM production in mouse ONH astrocytes.

2. Methods

2.1. Mouse ONH astrocyte isolation and culture

Maintenance and treatment of animals adhered to the institutional guidelines for the humane treatment of animals (IACUC #473) and to the ARVO Statement for the Use of Animals in Ophthalmic and Vision Research. Isolation of primary mouse ONH astrocytes was performed according to protocols modified from Zhao et al. (Zhao et al., 2017) and Mandal et al. (Mandal et al., 2010). Briefly, C57BL/6J mice were purchased from the Jackson Laboratory (Bar Harbor, ME). Six mice aged 6–8 weeks were used for each isolation. Using a SMZ1270 stereomicroscope (Nikon Instruments, Melville, NY), ONH tissue was dissected from each globe proximal to the sclera, with care to discard as much myelinated optic nerve tissue and peripapillary sclera as possible. ONH samples were digested for 15 min using 0.25% trypsin (Invitrogen, 25200-056, Carlsbad, CA) at 37 °C and resuspended in ONH astrocyte growth medium (Dulbecco's modified Eagle's medium), DMEM/F12 (Invitrogen, 11330-032) + 10% fetal bovine serum (Atlanta Biologicals, S11550, Atlanta, GA) + 1% penicillin/streptomycin (Corning, 30-001-CI, Manassas, VA) + 1% Glutamax (Invitrogen, 35050-061) + 25 ng/ml epidermal growth factor (Sigma, E4127-5X, St. Louis,

MO). ONH tissue was then plated in cell culture flasks coated with 0.2% gelatin (Sigma, G1393) and maintained at 37 °C in a humidified atmosphere with 5% CO_2. ONH astrocytes were allowed to migrate from the tissue and were passaged after 10–14 days. Three separate cultures were used for the experiments within this study at passages 2–5.

2.2. ONH astrocyte characterization

ONH astrocytes were seeded at 1×10^4 cells/cm^2 on sterilized glass coverslips in 24-well culture plates (Thermo Fisher Scientific, Waltham, MA). After 48 h, cells were fixed with 4% paraformaldehyde (PFA; J19943-K2, Thermo Fisher Scientific) at room temperature for 10 min, and permeabilized with 0.5% Triton X-100 (Thermo Fisher Scientific, 85111) at room temperature for 30 min. Cells were washed in Dulbecco's Phosphate Buffered Saline 1X (DPBS; Invitrogen, 14190-44) and blocked (PowerBlock; Biogenx, HK085–5K, San Ramon, CA) for 1 h at room temperature. Cells were then incubated for 1 h at room temperature with rabbit anti-glial fibrillary acidic protein (GFAP; 1:300; Dako, Z0334, Carpinteria, CA), rabbit anti-oligodendrocyte specific protein (OSP; 1:100; Abcam, Ab53041, Cambridge, MA) or rat anti-F4/80 (1:50; BioRad, MCA497GA, Hercules, CA). Cells were again washed in DPBS and incubated for 1 h at room temperature with Alexa Fluor® 488-conjugated secondary antibodies (1:500; Abcam, Ab150077, Invitrogen, A21208). Nuclei were counterstained with $4',6'$-diamidino-2-phenylindole (DAPI; Invitrogen, D1306). Coverslips were mounted with ProLong™ Gold Antifade (Thermo Fisher Scientific, P36930) on Superfrost™ Plus microscope slides (Fisher Scientific) and fluorescent images were acquired with an Eclipse N*i* microscope (Nikon). Four representative fields at 20x magnification were taken from each coverslip per culture; number of GFAP-, OSP-, or F4/80-positive cells versus total number of cells were quantified.

2.3. Cell treatments

ONH astrocytes were seeded at 1×10^4 cells/cm^2 on sterilized glass coverslips in 24-well culture plates (Thermo Fisher Scientific, Waltham, MA). After 24 h, cells were treated with increasing doses of TGFβ2 (vehicle control, 1.25 ng/ml, 2.5 ng/ml, and 5 ng/ml; R&D Systems, Minneapolis, MN) for 48 h. In a separate set of experiments, cells underwent the following treatments for 48 h: (1) vehicle control, (2) TGFβ2 (5 ng/ml), (3) TGFβ2 (5 ng/ml) + GsMTx4 (500 nM; Sigma-Aldrich), or (4) GsMTx4 (500 nM).

2.4. Staining for f-actin and analysis of cross-linked actin networks (CLANs)

After treatment for 48 h, coverslips were stained for filamentous factin as previously described (Li et al., 2021). Briefly, cells were fixed with 4% PFA, permeabilized with 0.5% Triton™ X-100, and stained with Phalloidin-iFluor 488 (Cell Signaling Technology, 12935S) according to the manufacturer's instructions. Nuclei were counterstained with DAPI, and fluorescent images were acquired with an Eclipse N*i* microscope (Nikon). Ten representative images were obtained at 60x magnification for each coverslip. CLANs were identified according to established protocols (Hoare et al., 2009; Filla et al., 2011). Specifically, CLANs were identified by their geodesic architecture with triangulation between f-actin spokes and hubs; a minimum of 3–5 hubs was necessary for identification of a CLAN. The number of CLAN-positive cells versus total number of cells was quantified.

2.5. Staining and fluorescence quantification of GFAP, fibronectin, and collagen IV immunoreactivity

Cells were immunostained for GFAP (rabbit anti-GFAP, 1:300, Dako), fibronectin (rabbit anti-fibronectin antibody, 1:500, Abcam, Ab45688), and collagen IV (rabbit anti-collagen IV (1:250, Abcam, Ab6586)) as detailed in *Methods 2.2.* Fluorescence intensity was quantified in four fields at 20x magnification per coverslip with background subtraction using Fiji software (NIH, Bethesda, MD).

2.6. Immunoblotting and analysis

ONH astrocytes in 6-well plates were treated, washed with ice-cold 1X DPBS (Gibco, Thermo Fisher Scientific), and lysates were scraped into 2X Laemmli sample buffer (90% sample buffer, 10% β-mercaptoethanol (BME; Fisher Chemical, 034461-100)). Samples were boiled for 5 min, loaded in equal amounts (10 μg) into NuPAGETM 4–12% Bis-Tris Gels (Invitrogen; NP0321), and proteins separated using SDS-PAGE at a constant rate of 180 V for 80 (+30) min. Proteins in gel slabs were transferred electrophoretically to 0.45 μm nitrocellulose Immobilon-FL membranes (Sigma; IPFL00010). Membranes were blocked with 5% bovine serum albumin (Thermo Fisher Scientific; BP9706) in trisbuffered saline with 0.2% Tween®20 (Thermo Fisher Scientific), and probed with primary antibodies against GFAP (rabbit polyclonal GFAP antibody, 1:1000; Novus Biologicals, NB300-141) and fibronectin (rabbit anti-fibronectin antibody, 1:50000, Abcam, Ab45688) followed by incubation with an IRDye 680RD goat-anti-rabbit secondary antibody (1:15000, LI-COR, 926–68071). Bound antibodies were visualized using the Li-Cor Odyssey CLx Infrared imaging system. Densitometry of target antibody bands was performed using ImageStudioLite software and normalized to correspondent GAPDH bands (anti-GAPDH [G9545] 1:80000; Sigma-Aldrich).

2.7. Statistical analysis

Individual sample sizes are specified in each figure caption. Comparisons between groups were assessed by one-way analysis of variance (ANOVA) with Tukey's multiple comparisons *post hoc* tests, as appropriate. All data are shown with mean ± SD, some with individual data points. For CLAN quantification, each data point represents the mean of 10 fields of view per experiment (N = 10). For fluorescence quantification, each data point represents the total fluorescence intensity – background intensity for 4 separate fields of view per experiment (N = 9). The significance level was set at $p < 0.05$ or lower. GraphPad Prism software v9.1 (GraphPad Software, La Jolla, CA, USA) was used for all analyses.

3. Results

3.1. ONH astrocyte characterization

Primary ONH astrocytes were derived from C57BL/6J mice aged 6–8 weeks using previously described methods (Mandal et al., 2010; Zhao et al., 2017). Cells were ~97% positive for the astrocyte marker GFAP, and effectively negative for markers of oligodendrocytes or microglia (~3–5%) (Supp. Fig. 1), thereby identifying them as ONH astrocytes.

3.2. TGFβ2 treatment induces actin cytoskeletal disorganization and CLAN formation in ONH astrocytes

Levels of TGFβ2 are increased within the glaucomatous ONH (Pena et al., 1999). Since TGFβ2 induces actin cytoskeletal reorganization in other ocular tissues (Fuchshofer and Tamm, 2012; Montecchi-Palmer et al., 2017), we asked whether exogenous treatment of TGFβ2 would exert similar effects on cultured mouse ONH astrocytes.

Vehicle control-treated astrocytes demonstrated baseline organization of the f-actin network (Fig. 1A). Treatment with TGFβ2 altered f-actin fiber morphology (Fig. 1B–D). Specifically, we observed focal areas of disorganized actin fibers, akin to the cross-linked actin networks (CLANs) seen in glaucomatous trabecular meshwork cells (insets Fig. 1C & D). To our knowledge, this is the first description of CLAN formation within ONH astrocytes. We found a significant increase in CLAN-containing cells in a dose-dependent manner (Fig. 1E). Treatment with 5 ng/ml TGFβ2 resulted in CLAN formation within ~25% ONH astrocytes; thus 5 ng/ml TGFβ2 was selected for all future treatments.

3.3. Co-treatment with a mechanosensitive channel inhibitor reduces TGFβ2-mediated actin cytoskeletal disorganization and CLAN formation in ONH astrocytes

Mechanosensitive channels are critical for cells to sense and respond to external stimuli (Petho et al., 2019). Therefore, we tested whether co-treatment with the nonspecific mechanosensitive channel inhibitor GsMTx4 (Gnanasambandam et al., 2017) would ameliorate TGFβ2-mediated actin cytoskeletal disorganization in ONH astrocytes.

Again, minimal CLANs were visualized in vehicle control-treated cells (Fig. 2A), while increased f-actin stress fibers and significant CLANs were noted in cells treated with TGFβ2 (Fig. 2B,E). Co-treatment with TGFβ2 and GsMTx4 resulted in f-actin fiber orientation similar to vehicle control-treated cells, and a significantly decreased percentage of CLANs vs. TGFβ2 (12% vs. 25%, $p < 0.001$) (Fig. 2C,E). Lastly, treatment with GsMTx4 also resulted in f-actin fiber morphology comparable to control cells (Fig. 2D and E). These data suggest that mechanosensitive channel inhibition has the potential to modify the ONH astrocyte actin cytoskeleton in response to a glaucomatous stressor.

3.4. Co-treatment with a mechanosensitive channel inhibitor reduces TGFβ2-mediated GFAP immunoreactivity in ONH astrocytes

Astrocytes within the glaucomatous ONH develop reactive gliosis, associated with changes in their morphology and transcriptional behavior (Sun et al., 2017). Therefore, we asked whether mechanosensitive channel inhibition would attenuate TGFβ2-stimulated reactive gliosis in ONH astrocytes.

ONH astrocytes treated with vehicle control for 48 h demonstrated low baseline levels of GFAP expression (Fig. 3A and B). Treatment with TGFβ2 induced a significant ~20% increase in GFAP immunofluorescence intensity in cells exposed to TGFβ2 vs. controls ($p < 0.0001$) (Fig. 3A and B), while co-treatment with GsMTx4 significantly ameliorated the response to TGFβ2, with GFAP intensity returning to baseline levels (Fig. 3A and B).

Treatment of ONH astrocytes with GsMTx4 alone resulted in GFAP levels similar to vehicle control (Fig. 3A and B).

We then confirmed these alterations in GFAP through immunoblotting analyses. Similar trends were observed. Treatment of ONH astrocytes with TGFβ2 resulted in increased levels of GFAP, while cotreatment with GsMTx4 decreased GFAP levels (Fig. 3C). Densitometry analysis mirrored these trends, but did not show a significant fold change (Fig. 3D).

3.5. Co-treatment with a mechanosensitive channel inhibitor does not alter short-term TGFβ2-mediated fibronectin and collagen IV production by ONH astrocytes

TGFβ2 treatment of ONH astrocytes directly induces production/secretion of fibronectin and collagen IV (Fuchshofer et al., 2005), which may contribute to overall ECM changes within the ONH. Therefore, we tested whether mechanosensitive channel inhibition would prevent TGFβ2-induced upregulation of ECM proteins by ONH astrocytes.

Vehicle control treated ONH astrocytes displayed low levels of fibronectin expression (Fig. 4A and B). Treatment with TGFβ2 for 48 h resulted in a significant ~75% increase in fibronectin intensity vs. controls ($p < 0.05$) (Fig. 4A and B). Co-treatment of TGFβ2 and GsMTx4 did not change fibronectin levels (Fig. 4A and B). Treatment with GsMTx4 alone resulted in fibronectin intensity similar to vehicle controls (Fig. 4A and B). Immunoblotting analyses revealed no effect of GsMTx4 co-treatment on TGFβ2-induced fibronectin production (Fig. 4C and D).

We then tested whether mechanosensitive channel inhibition would alter production of another ECM protein, collagen IV. Again, treatment with TGFβ2 increased collagen IV immunoreactivity by ~80% ($p < 0.0001$) (Fig. 5A and B). Co-treatment of GsMTx4 did not alter TGFβ2-mediated induction of collagen IV (Fig. 5A and B).

4. Discussion

Glaucoma is a multifactorial disease, and several mechanisms contribute to eventual retinal ganglion cell dysfunction/loss. Astrocytes have been identified as key responders to glaucomatous insult (Hernandez, 2000; Sun et al., 2017; Cooper et al., 2020). In neural tissues, astrocytes modulate synapse formation and mediate metabolic stressors; they are also capable of directing scar formation and remodeling the surrounding ECM (Blanco-Suarez et al., 2017). Within the ONH, astrocyte mobility and reactivity has been shown to promote ganglion cell viability (Sun et al., 2017; Cooper et al., 2020). In certain cases, however, astrocytes may adopt a more detrimental phenotype, becoming neurotoxic (Liddelow et al., 2017; Sterling et al., 2020), and later in the disease, ONH astrocytes elicit fibrosis of the surrounding ECM, which negatively affects ganglion cell health (Schneider and Fuchshofer, 2016). Our overall aim, then, is to elucidate mechanisms governing the complex ONH astrocyte response to glaucomatous stressors, with the ultimate goal of precisely directing ONH astrocyte behavior to best preserve ganglion cell function and viability.

Aging and elevated intraocular pressure are the highest correlated risk factors for glaucoma (Weinreb et al., 2014). Age-associated stiffening of the outflow pathway within the eye may induce elevated intraocular pressure in susceptible individuals, and this stiffening is linked to increased TGFβ2 levels in that region (Agarwal et al., 2015). Similarly, TGFβ2 levels are elevated within ONH astrocytes in glaucoma, which may play a role in ONH fibrosis seen in end-stage disease (Pena et al., 1999). What is not known, however, is the precise mechanisms governing TGFβ2-induced astrocyte actin cytoskeletal changes in glaucoma. In the current study, we demonstrate that TGFβ2 treatment of ONH astrocytes elicits alterations to the actin cytoskeleton and reactive gliosis in a mechanosensitive channel-dependent manner.

Alteration of the f-actin cytoskeleton within ONH astrocytes has been demonstrated in response to elevated IOP in vivo and elevated hydrostatic pressure in vitro (Ricard et al., 2000; Tehrani, Davis et al. 2016, 2019; Ling et al., 2020). In our study, treatment with TGFβ2 increased actin stress fibers in ONH astrocytes, similar to what is observed in trabecular meshwork cells within the outflow system of the eye (O'Reilly et al., 2011), demonstrating the clear potential of TGFβ2 to modulate the ONH astrocyte actin cytoskeleton. Interestingly, we also visualized CLANs (Fig. 1), unique actin arrangements, within ONH astrocytes after treatment. In a single targeted analysis of human optic nerve head tissue, CLANs were not visualized within control nor glaucomatous ONH astrocytes (Job et al., 2010).

Our data additionally confirmed that TGFβ2 induces ONH astrocyte reactivity (Fig. 3), fibronectin, and collagen IV production (Figs. 4 and 5). ONH astrocyte reactivity is well-documented in response to glaucomatous stressors, including elevated IOP, oxidative stress, and TGFβ2 (Tezel et al., 2001; Yu et al., 2009; Zode et al., 2011; Sun et al., 2013; Kim et al., 2017; Zhao et al., 2021). Several mechanisms have been implicated in glaucomatous ONH astrocyte reactivity, including vasoactive factors such as endothelin-1 and inducible nitric oxide synthase (Liu and Neufeld, 2000; Prasanna et al., 2011). Here, we showed that mechanosensitive channel activity is an additional mechanism through which glaucomatous stressors induce ONH astrocyte reactivity.

Co-treatment with the mechanosensitive channel inhibitor GsMTx4 potently reduced TGFβ2-induced actin cytoskeletal dysregulation and CLAN formation (Fig. 2) within a short time-frame (48 h) after exposure to TGFβ2. In addition, GsMTx4 co-treatment reversed TGFβ2-induced reactive gliosis (Fig. 3), which likely modulates retinal ganglion cell viability in glaucoma. Interestingly, mechanosensitive channel inhibition did not appear to affect TGFβ2-induced ECM production after 48 h (Figs. 4 and 5). Long-term experiments will be needed to examine the role of mechanosensitive channel activity on optic nerve fibrosis in glaucoma.

The studies described herein are among the earliest to highlight the role of mechanosensitive channels in modulating the ONH astrocyte response to glaucomatous stressors. GsMTx4 is a relatively nonselective inhibitor of cationic mechanosensitive channels, which include calcium, sodium, and potassium channels (Gnanasambandam et al., 2017). Of these, calcium channels are attractive candidate mediators of actin fiber realignment since calcium can

directly modulate the actin cytoskeleton (Hepler, 2016). One particular caveat of using such a nonselective channel inhibitor is that further research is needed to identify which mechanosensitive channels modulate TGFβ2 regulation of the actin cytoskeleton and reactive gliosis. Attractive candidates include Piezo and TRP channels, both of which have implicated in the retinal and ONH response to insult. Previous studies have shown that intraocular pressure elevation in murine models of glaucoma upregulates mechanosensitive channel expression (Choi et al., 2015), and that mechanical stretch increases Piezo1 activity in ONH astrocytes (Liu et al., 2021). Piezo1/2 localized to retinal ganglion cell soma and Piezo2 increased in response to elevated IOP, supporting its role in glaucoma pathogenesis (Morozumi et al., 2020). Of the TRP channels, absence of TRPA1 protected retinal ganglion cells in response to ischemia/reperfusion injury (Souza Monteiro de Araujo, De Logu et al., 2020). Additionally, TRPV4 stimulation promoted retinal ganglion cell apoptosis in response to hypotonic strain and absence of TRPV1 potentiated optic nerve damage in response to elevated IOP (Ryskamp et al., 2011; Ward et al., 2014). As such, there are several candidate mechanosensitive channels that may mediate TGFβ2-induced actin cytoskeletal remodeling and reactivity in ONH astrocytes; future studies will use targeted knockdown analyses and pharmacologic inhibition to identify which mechanosensitive channels are involved.

In conclusion, this study identifies inhibition of mechanosensitive channels as an attractive means to modulate ONH astrocyte behavior in glaucoma. Our data support that mechanosensitive channel inhibition ameliorates features of glaucomatous astrocyte response (i.e., actin cytoskeletal dysregulation and reactive gliosis). As astrocytes are a primary support cell to retinal ganglion cells, it is not yet known how these changes in astrocyte behavior will ultimately affect ganglion cell function. Additional work in our laboratory will explore the impact of astrocyte mechanosensitive channel function on retinal ganglion cell health and function.

Supplementary Material

Refer to Web version on PubMed Central for supplementary material.

Acknowledgments

Data and materials availability

All data needed to evaluate the conclusions in the paper are present in the paper. Additional data related to this paper may be requested from the authors.

References

Agarwal P, Daher AM, Agarwal R, 2015. Aqueous humor TGF-beta2 levels in patients with open-angle glaucoma: a meta-analysis. Mol. Vis 21, 612–620. [PubMed: 26019480]

Anderson DR, Hendrickson A, 1974. Effect of intraocular pressure on rapid axoplasmic transport in monkey optic nerve. Invest. Ophthalmol 13 (10), 771–783. [PubMed: 4137635]

Blanco-Suarez E, Caldwell AL, Allen NJ, 2017. Role of astrocyte-synapse interactions in CNS disorders. J. Physiol 595 (6), 1903–1916. [PubMed: 27381164]

Chen X, Wanggou S, Bodalia A, Zhu M, Dong W, Fan JJ, Yin WC, Min HK, Hu M, Draghici D, Dou W, Li F, Coutinho FJ, Whetstone H, Kushida MM, Dirks PB, Song Y, Hui CC, Sun Y, Wang LY, Li X, Huang X, 2018. A feedforward mechanism mediated by mechanosensitive ion channel PIEZO1 and tissue mechanics promotes glioma aggression. Neuron 100 (4), 799–815 e797. [PubMed: 30344046]

Choi HJ, Sun D, Jakobs TC, 2015. Astrocytes in the optic nerve head express putative mechanosensitive channels. Mol. Vis 21, 749–766. [PubMed: 26236150]

Cooper ML, Collyer JW, Calkins DJ, 2018. Astrocyte remodeling without gliosis precedes optic nerve Axonopathy. Acta Neuropathol. Commun 6 (1), 38. [PubMed: 29747701]

Cooper ML, Pasini S, Lambert WS, D'Alessandro KB, Yao V, Risner ML, Calkins DJ, 2020. Redistribution of metabolic resources through astrocyte networks mitigates neurodegenerative stress. Proc. Natl. Acad. Sci. U. S. A 117 (31), 18810–18821. [PubMed: 32690710]

Crawford Downs J, Roberts MD, Sigal IA, 2011. Glaucomatous cupping of the lamina cribrosa: a review of the evidence for active progressive remodeling as a mechanism. Exp. Eye Res 93 (2), 133–140. [PubMed: 20708001]

Filla MS, Schwinn MK, Nosie AK, Clark RW, Peters DM, 2011. Dexamethasone-associated cross-linked actin network formation in human trabecular meshwork cells involves beta3 integrin signaling. Invest. Ophthalmol. Vis. Sci 52 (6), 2952–2959. [PubMed: 21273548]

Fuchshofer R, Birke M, Welge-Lussen U, Kook D, Lutjen-Drecoll E, 2005. Transforming growth factor-beta 2 modulated extracellular matrix component expression in cultured human optic nerve head astrocytes. Invest. Ophthalmol. Vis. Sci 46 (2), 568–578. [PubMed: 15671284]

Fuchshofer R, Tamm ER, 2012. The role of TGF-beta in the pathogenesis of primary open-angle glaucoma. Cell Tissue Res. 347 (1), 279–290. [PubMed: 22101332]

Gnanasambandam R, Ghatak C, Yasmann A, Nishizawa K, Sachs F, Ladokhin AS, Sukharev SI, Suchyna TM, 2017. GsMTx4: mechanism of inhibiting mechanosensitive ion channels. Biophys. J 112 (1), 31–45. [PubMed: 28076814]

Hepler PK, 2016. The cytoskeleton and its regulation by calcium and protons. Plant Physiol. 170 (1), 3–22. [PubMed: 26722019]

Hernandez MR, 2000. The optic nerve head in glaucoma: role of astrocytes in tissue remodeling. Prog. Retin. Eye Res 19 (3), 297–321. [PubMed: 10749379]

Hernandez MR, Igoe F, Neufeld AH, 1988. Cell culture of the human lamina cribrosa. Invest. Ophthalmol. Vis. Sci 29 (1), 78–89. [PubMed: 3275593]

Hernandez MR, Luo XX, Igoe F, Neufeld AH, 1987. Extracellular matrix of the human lamina cribrosa. Am. J. Ophthalmol 104 (6), 567–576. [PubMed: 3318474]

Hoare MJ, Grierson I, Brotchie D, Pollock N, Cracknell K, Clark AF, 2009. Cross-linked actin networks (CLANs) in the trabecular meshwork of the normal and glaucomatous human eye in situ. Invest. Ophthalmol. Vis. Sci 50 (3), 1255–1263. [PubMed: 18952927]

Hopkins AA, Murphy R, Irnaten M, Wallace DM, Quill B, O'Brien C, 2020. The role of lamina cribrosa tissue stiffness and fibrosis as fundamental biomechanical drivers of pathological glaucoma cupping. Am. J. Physiol. Cell Physiol 319 (4), C611–C623. [PubMed: 32667866]

Howell GR, Libby RT, Jakobs TC, Smith RS, Phalan FC, Barter JW, Barbay JM, Marchant JK, Mahesh N, Porciatti V, Whitmore AV, Masland RH, John SW, 2007. Axons of retinal ganglion cells are insulted in the optic nerve early in DBA/2J glaucoma. J. Cell Biol 179 (7), 1523–1537. [PubMed: 18158332]

Job R, Raja V, Grierson I, Currie L, O'Reilly S, Pollock N, Knight E, Clark AF, 2010. Cross-linked actin networks (CLANs) are present in lamina cribrosa cells. Br. J. Ophthalmol 94 (10), 1388–1392. [PubMed: 20693558]

Kim ML, Sung KR, Shin JA, Young Yoon J, Jang J, 2017. Statins reduce TGF-beta2-modulation of the extracellular matrix in cultured astrocytes of the human optic nerve head. Exp. Eye Res 164, 55–63. [PubMed: 28789942]

Li H, Bague T, Kirschner A, Strat AN, Roberts H, Weisenthal RW, Patteson AE, Annabi N, Stamer WD, Ganapathy PS, Herberg S, 2021. A tissue-engineered human trabecular meshwork hydrogel for advanced glaucoma disease modeling. Exp. Eye Res 205, 108472. [PubMed: 33516765]

Liddelow SA, Guttenplan KA, Clarke LE, Bennett FC, Bohlen CJ, Schirmer L, Bennett ML, Munch AE, Chung WS, Peterson TC, Wilton DK, Frouin A, Napier BA, Panicker N, Kumar M, Buckwalter MS, Rowitch DH, Dawson VL, Dawson TM, Stevens B, Barres BA, 2017. Neurotoxic reactive astrocytes are induced by activated microglia. Nature 541 (7638), 481–487. [PubMed: 28099414]

Ling YTT, Pease ME, Jefferys JL, Kimball EC, Quigley HA, Nguyen TD, 2020. Pressure-induced changes in astrocyte GFAP, actin, and nuclear morphology in mouse optic nerve. Invest. Ophthalmol. Vis. Sci 61 (11), 14.

Liu B, McNally S, Kilpatrick JI, Jarvis SP, O'Brien CJ, 2018. Aging and ocular tissue stiffness in glaucoma. Surv. Ophthalmol 63 (1), 56–74. [PubMed: 28666629]

Liu B, Neufeld AH, 2000. Expression of nitric oxide synthase-2 (NOS-2) in reactive astrocytes of the human glaucomatous optic nerve head. Glia 30 (2), 178–186. [PubMed: 10719359]

Liu J, Yang Y, Liu Y, 2021. Piezo1 plays a role in optic nerve head astrocyte reactivity. Exp. Eye Res 204, 108445. [PubMed: 33465396]

Mandal A, Shahidullah M, Delamere NA, 2010. Hydrostatic pressure-induced release of stored calcium in cultured rat optic nerve head astrocytes. Invest. Ophthalmol. Vis. Sci 51 (6), 3129–3138. [PubMed: 20071675]

May CA, Lutjen-Drecoll E, 2002. Morphology of the murine optic nerve. Invest. Ophthalmol. Vis. Sci 43 (7), 2206–2212. [PubMed: 12091418]

Montecchi-Palmer M, Bermudez JY, Webber HC, Patel GC, Clark AF, Mao W, 2017. TGFbeta2 induces the formation of cross-linked actin networks (CLANs) in human trabecular meshwork cells through the smad and non-smad dependent pathways. Invest. Ophthalmol. Vis. Sci 58 (2), 1288–1295. [PubMed: 28241317]

Morozumi W, Inagaki S, Iwata Y, Nakamura S, Hara H, Shimazawa M, 2020. Piezo channel plays a part in retinal ganglion cell damage. Exp. Eye Res 191, 107900. [PubMed: 31874142]

Morrison JC, Cepurna Ying Guo WO, Johnson EC, 2011. Pathophysiology of human glaucomatous optic nerve damage: insights from rodent models of glaucoma. Exp. Eye Res 93 (2), 156–164. [PubMed: 20708000]

Morrison JC, Jerdan JA, L'Hernault NL, Quigley HA, 1988. The extracellular matrix composition of the monkey optic nerve head. Invest. Ophthalmol. Vis. Sci 29 (7), 1141–1150. [PubMed: 3047074]

O'Reilly S, Pollock N, Currie L, Paraoan L, Clark AF, Grierson I, 2011. Inducers of cross-linked actin networks in trabecular meshwork cells. Invest. Ophthalmol. Vis. Sci 52 (10), 7316–7324. [PubMed: 21849423]

Pena JD, Taylor AW, Ricard CS, Vidal I, Hernandez MR, 1999. Transforming growth factor beta isoforms in human optic nerve heads. Br. J. Ophthalmol 83 (2), 209–218. [PubMed: 10396201]

Petho Z, Najder K, Bulk E, Schwab A, 2019. Mechanosensitive ion channels push cancer progression. Cell Calcium 80, 79–90. [PubMed: 30991298]

Pijanka JK, Markov PP, Midgett D, Paterson NG, White N, Blain EJ, Nguyen TD, Quigley HA, Boote C, 2019. Quantification of collagen fiber structure using second harmonic generation imaging and two-dimensional discrete Fourier transform analysis: application to the human optic nerve head. J. Biophot 12 (5), e201800376.

Prasanna G, Krishnamoorthy R, Yorio T, 2011. Endothelin, astrocytes and glaucoma. Exp. Eye Res 93 (2), 170–177. [PubMed: 20849847]

Quigley H, Anderson DR, 1976. The dynamics and location of axonal transport blockade by acute intraocular pressure elevation in primate optic nerve. Invest. Ophthalmol 15 (8), 606–616. [PubMed: 60300]

Quigley HA, Broman AT, 2006. The number of people with glaucoma worldwide in 2010 and 2020. Br. J. Ophthalmol 90 (3), 262–267. [PubMed: 16488940]

Quigley HA, Guy J, Anderson DR, 1979. Blockade of rapid axonal transport. Effect of intraocular pressure elevation in primate optic nerve. Arch. Ophthalmol 97 (3), 525–531. [PubMed: 84662]

Ricard CS, Kobayashi S, Pena JD, Salvador-Silva M, Agapova O, Hernandez MR, 2000. Selective expression of neural cell adhesion molecule (NCAM)-180 in optic nerve head astrocytes exposed to elevated hydrostatic pressure in vitro. Brain Res. Mol. Brain Res 81 (1–2), 62–79. [PubMed: 11000479]

Ryskamp DA, Witkovsky P, Barabas P, Huang W, Koehler C, Akimov NP, Lee SH, Chauhan S, Xing W, Renteria RC, Liedtke W, Krizaj D, 2011. The polymodal ion channel transient receptor potential vanilloid 4 modulates calcium flux, spiking rate, and apoptosis of mouse retinal ganglion cells. J. Neurosci 31 (19), 7089–7101. [PubMed: 21562271]

Schneider M, Fuchshofer R, 2016. The role of astrocytes in optic nerve head fibrosis in glaucoma. Exp. Eye Res 142, 49–55. [PubMed: 26321510]

Souza Monteiro de Araujo D, De Logu F, Adembri C, Rizzo S, Janal MN, Landini L, Magi A, Mattei G, Cini N, Pandolfo P, Geppetti P, Nassini R, Calaza KDC, 2020. TRPA1 mediates damage of the retina induced by ischemia and reperfusion in mice. Cell Death Dis. 11 (8), 633. [PubMed: 32801314]

Sterling JK, Adetunji MO, Guttha S, Bargoud AR, Uyhazi KE, Ross AG, Dunaief JL, Cui QN, 2020. GLP-1 receptor agonist NLY01 reduces retinal inflammation and neuron death secondary to ocular hypertension. Cell Rep. 33 (5), 108271. [PubMed: 33147455]

Sun D, Moore S, Jakobs TC, 2017. Optic nerve astrocyte reactivity protects function in experimental glaucoma and other nerve injuries. J. Exp. Med 214 (5), 1411–1430. [PubMed: 28416649]

Sun D, Qu J, Jakobs TC, 2013. Reversible reactivity by optic nerve astrocytes. Glia 61 (8), 1218–1235. [PubMed: 23650091]

Tehrani S, Davis L, Cepurna WO, Choe TE, Lozano DC, Monfared A, Cooper L, Cheng J, Johnson EC, Morrison JC, 2016. Astrocyte structural and molecular response to elevated intraocular pressure occurs rapidly and precedes axonal tubulin rearrangement within the optic nerve head in a rat model. PLoS One 11 (11), e0167364. [PubMed: 27893827]

Tehrani S, Davis L, Cepurna WO, Delf RK, Lozano DC, Choe TE, Johnson EC, Morrison JC, 2019. Optic nerve head astrocytes display axon-dependent and -independent reactivity in response to acutely elevated intraocular pressure. Invest. Ophthalmol. Vis. Sci 60 (1), 312–321. [PubMed: 30665231]

Tezel G, Hernandez MR, Wax MB, 2001. In vitro evaluation of reactive astrocyte migration, a component of tissue remodeling in glaucomatous optic nerve head. Glia 34 (3), 178–189. [PubMed: 11329180]

Tham YC, Li X, Wong TY, Quigley HA, Aung T, Cheng CY, 2014. Global prevalence of glaucoma and projections of glaucoma burden through 2040: a systematic review and meta-analysis. Ophthalmology 121 (11), 2081–2090. [PubMed: 24974815]

Voorhees AP, Jan NJ, Austin ME, Flanagan JG, Sivak JM, Bilonick RA, Sigal IA, 2017. Lamina cribrosa pore shape and size as predictors of neural tissue mechanical insult. Invest. Ophthalmol. Vis. Sci 58 (12), 5336–5346. [PubMed: 29049736]

Ward NJ, Ho KW, Lambert WS, Weitlauf C, Calkins DJ, 2014. Absence of transient receptor potential vanilloid-1 accelerates stress-induced axonopathy in the optic projection. J. Neurosci 34 (9), 3161–3170. [PubMed: 24573275]

Weinreb RN, Aung T, Medeiros FA, 2014. The pathophysiology and treatment of glaucoma: a review. J. Am. Med. Assoc 311 (18), 1901–1911.

Yu AL, Moriniere J, Birke M, Neumann C, Fuchshofer R, Kampik A, Bloemendal H, Welge-Lussen U, 2009. Reactivation of optic nerve head astrocytes by TGF-beta2 and H2O2 is accompanied by increased Hsp32 and Hsp47 expression. Invest. Ophthalmol. Vis. Sci 50 (4), 1707–1717. [PubMed: 18952926]

Zhao J, Gonsalvez G, Bartoli M, Mysona BA, Smith SB, Bollinger KE, 2021. Sigma 1 receptor modulates optic nerve head astrocyte reactivity. Invest. Ophthalmol. Vis. Sci 62 (7), 5.

Zhao J, Mysona BA, Wang J, Gonsalvez GB, Smith SB, Bollinger KE, 2017. Sigma 1 receptor regulates ERK activation and promotes survival of optic nerve head astrocytes. PLoS One 12 (9), e0184421. [PubMed: 28898265]

Zode GS, Sethi A, Brun-Zinkernagel AM, Chang IF, Clark AF, Wordinger RJ, 2011. Transforming growth factor-beta2 increases extracellular matrix proteins in optic nerve head cells via activation of the Smad signaling pathway. Mol. Vis 17, 1745–1758. [PubMed: 21738403]
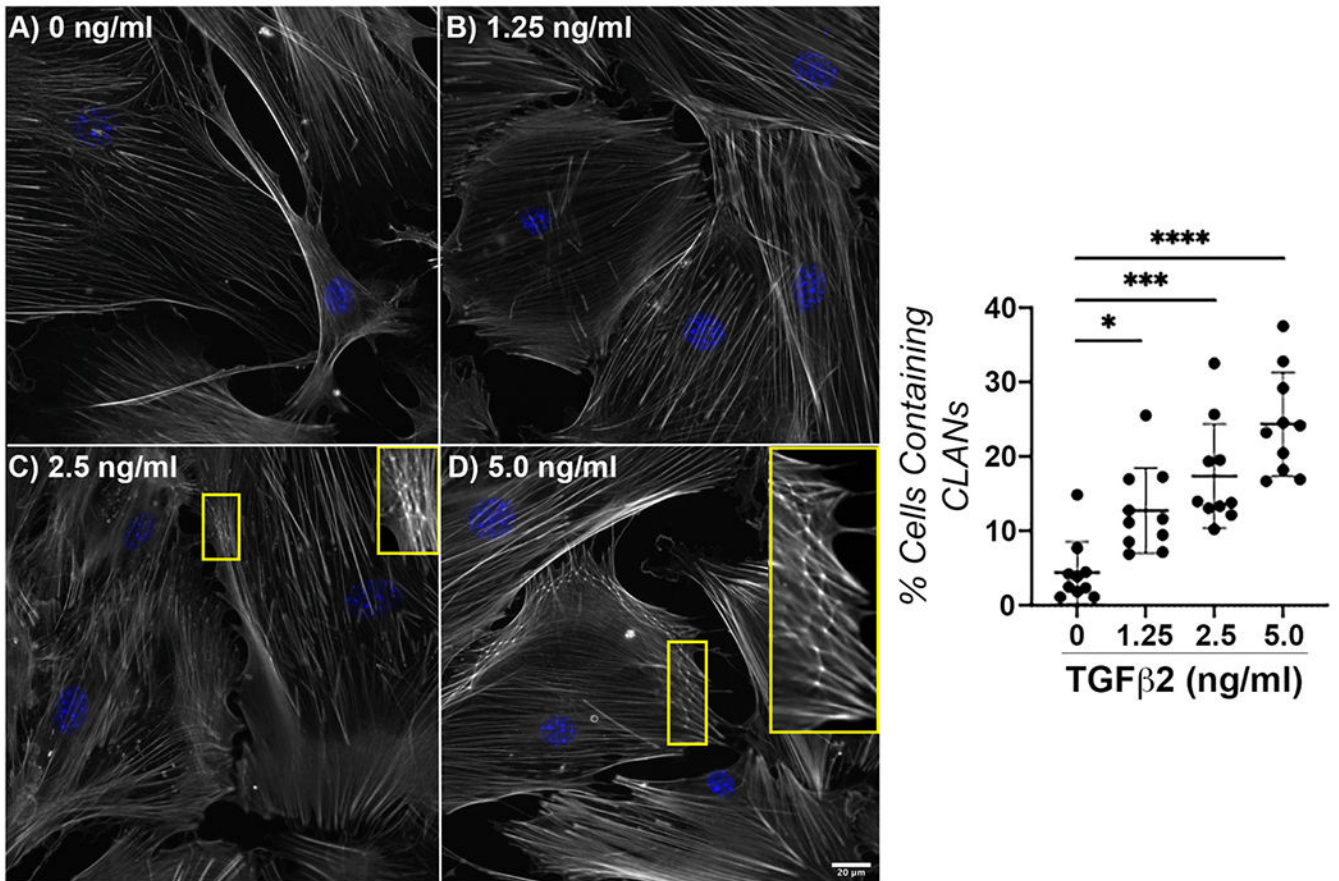
Fig. 1. Effect of TGFβ2 treatment on f-actin network.
Representative fluorescence images of f-actin within ONH astrocytes following treatment
with **(A)** vehicle control, **(B)** TGFβ2 (1.25 ng/ml), **(C)** TGFβ2 (2.5 ng/ml); inset magnified
view CLANs, and **(D)** TGFβ2 (5.0 ng/ml); inset CLANs for 48 h (f-actin = white, DAPI =
blue). Scale bar 20 μm. **(E)** Quantification of percent cells containing CLANs after TGFβ2
treatment for 48 h (vehicle control, 4.38 ± 4.18; 1.25 ng/ml, 12.72 ± 5.78; 2.5 ng/ml, 17.35 ±
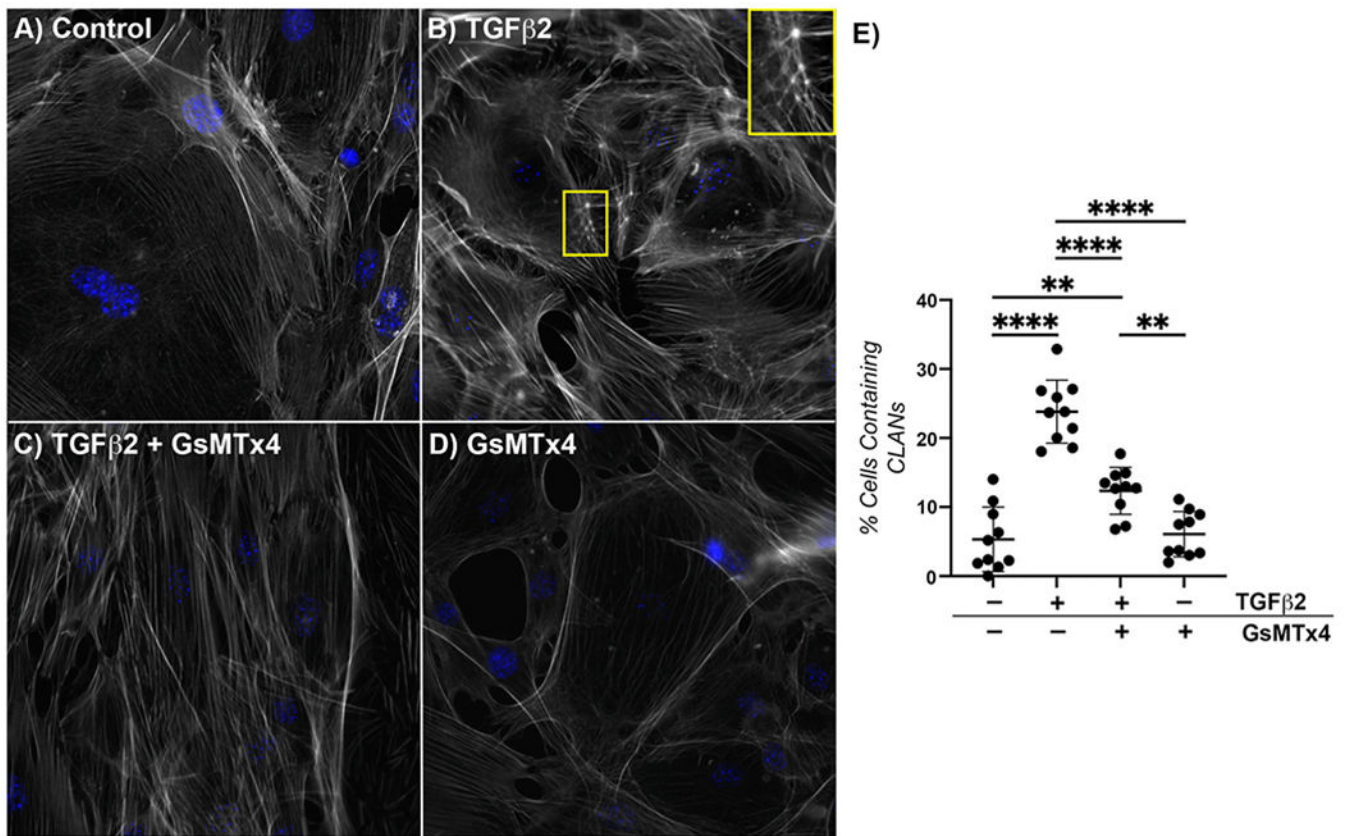7.02; 5.0 ng/ml, 24.35 ± 6.96; *p < 0.05; ***p < 0.001; ****p < 0.0001) N = 10.

Fig. 2. Effect of mechanosensitive channel inhibition on TGFβ2-induced f-actin dysregulation.
Representative fluorescence images of f-actin within ONH astrocytes following treatment
with **(A)** vehicle control, **(B)** TGFβ2 (5.0 ng/ml); inset CLAN, **(C)** TGFβ2 (5.0 ng/ml)
+ GsMTx4 (500 nM), and **(D)** GsMTx4 (500 nM) for 48 h (f-actin = white, DAPI =
blue). Scale bar 20 μm. **(E)** Quantification of percent cells containing CLANs after above
treatments for 48 h (vehicle control, 5.32 ± 4.65; TGFβ2, 23.83 ± 4.56; TGFβ2 + GsMTx4,
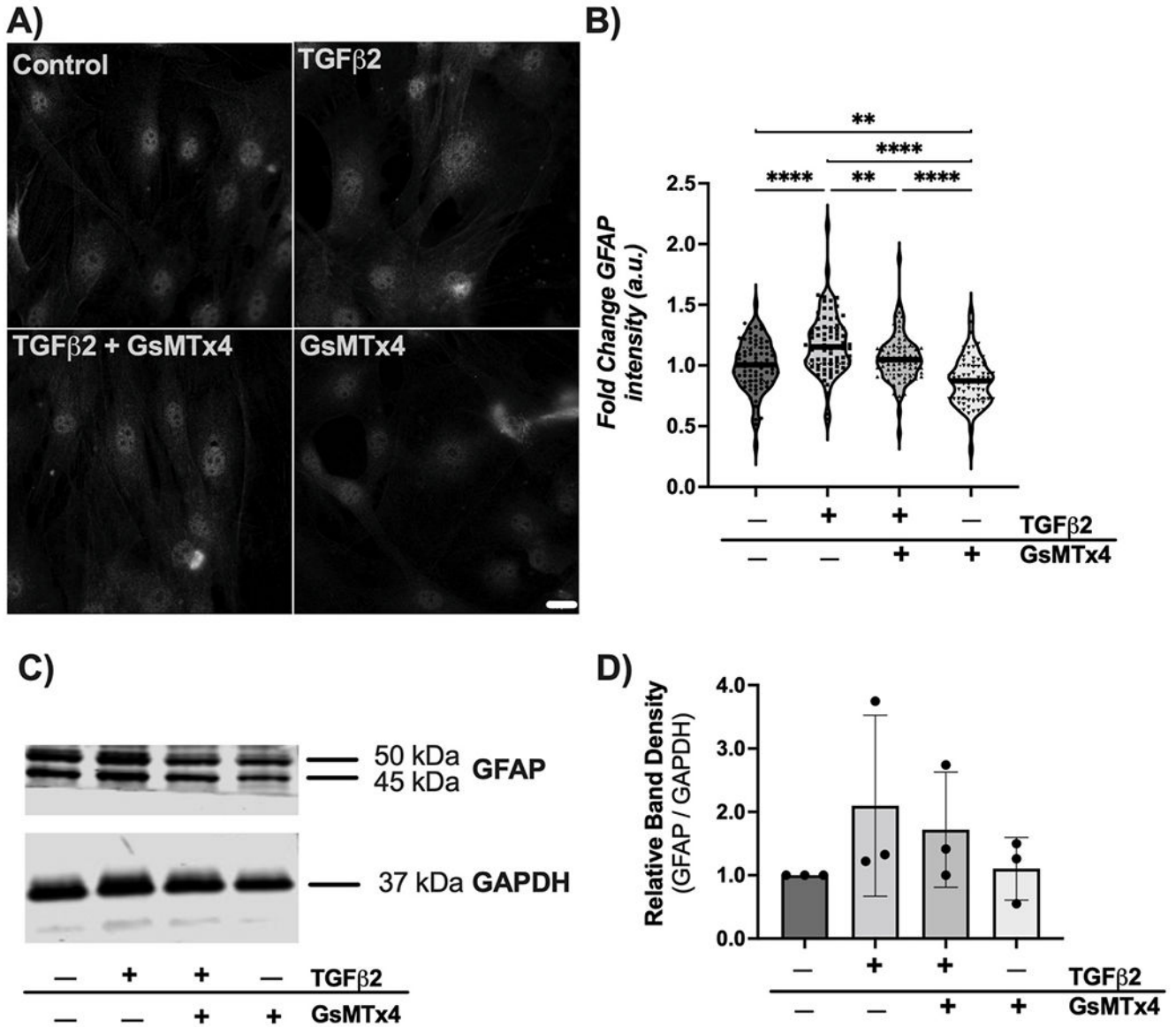12.36 ± 3.39; GsMTx4, 6.07 ± 3.29; **$p < 0.01$; ****$p < 0.0001$). N = 10.

Fig. 3. Effect of mechanosensitive channel inhibition on TGFβ2-induced GFAP immunoreactivity.

(A) Representative fluorescence images of GFAP within ONH astrocytes following treatment with vehicle control, TGFβ2 (5.0 ng/ml), TGFβ2 (5.0 ng/ml) + GsMTx4 (500 nM), and GsMTx4 (500 nM) for 48 h. Scale bar 20 μm. **(B)** Quantification of fold change in fluorescence intensity (mean ± SD, arbitrary units) after above treatments for 48 h (vehicle control, 1.00 ± 0.21; TGFβ2, 1.18 ± 0.25; TGFβ2 + GsMTx4, 1.06 ± 0.20; GsMTx4, 0.87 ± 0.20; **$p < 0.01$; ***$p < 0.001$; ****$p < 0.0001$). Data represent fluorescence quantification of 4 fields of view each for 9 separate experiments per group. **(C)** Representative immunoblot and (D) densitometry analysis (vehicle control 1.00 ± 0.00; TGFβ2, 2.10 ± 1.43; TGFβ2 + GsMTx4, 1.72 ± 0.91; GsMTx4, 1.10 ± 0.49).
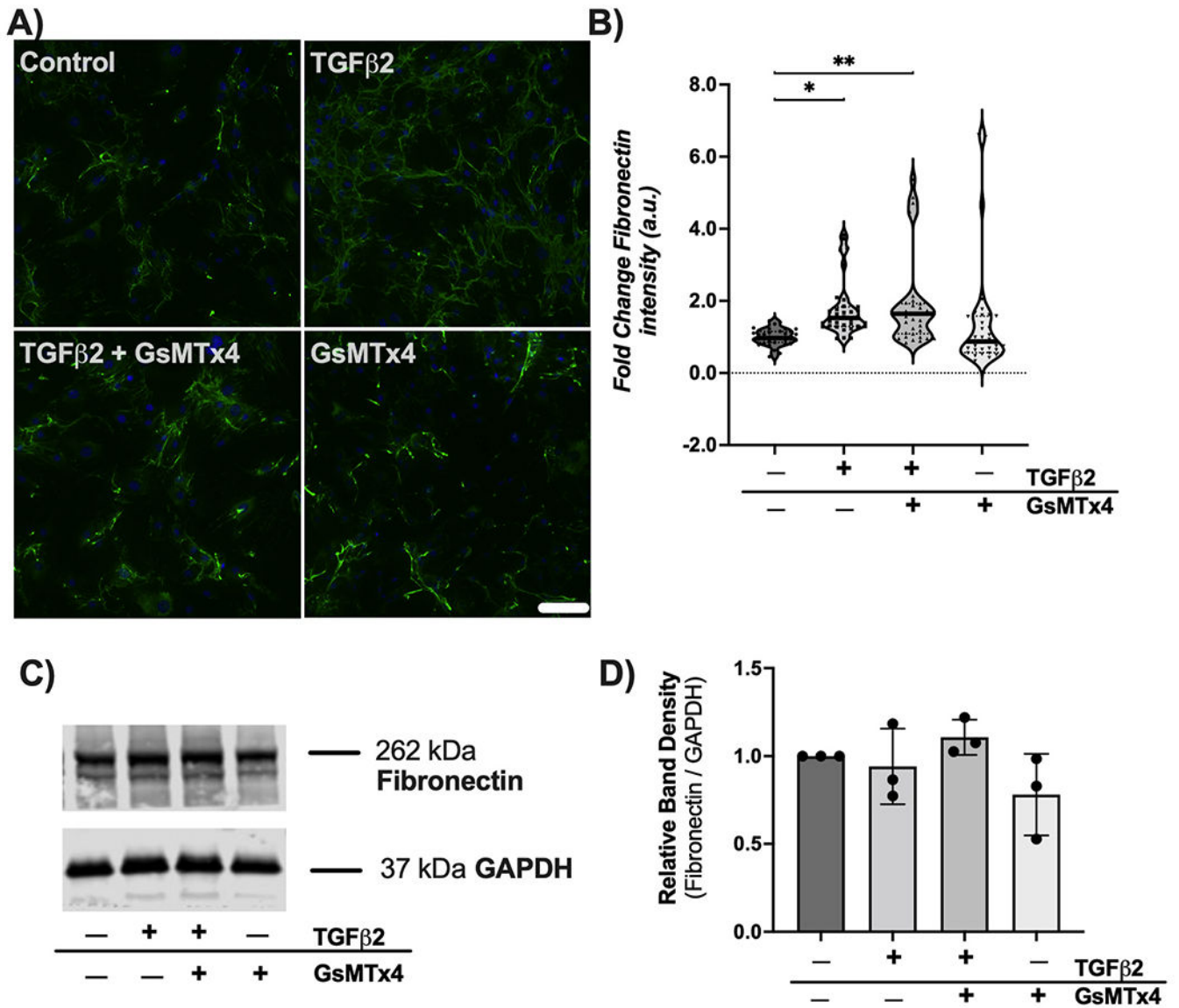
Fig. 4. Effect of mechanosensitive channel inhibition on TGFβ2-induced fibronectin immunoreactivity.

(A) Representative fluorescence images of fibronectin within ONH astrocytes following treatment with vehicle control, TGFβ2 (5.0 ng/ml), TGFβ2 (5.0 ng/ml) + GsMTx4 (500 nM), and GsMTx4 (500 nM) for 48 h (fibronectin = green, DAPI = blue. Scale bar 100 μm. **(B)** Quantification of fold change in fluorescence intensity (mean ± SD, arbitrary units) after above treatments for 48 h (vehicle control, 1.00 ± 0.23; TGFβ2, 1.76 ± 0.77; TGFβ2 + GsMTx4, 1.90 ± 1.25; GsMTx4, 1.38 ± 1.51; *$p < 0.05$; **$p < 0.01$). Data represent fluorescence quantification of 4 fields of view each for 9 separate experiments per group. **(C)** Representative immunoblot and (D) densitometry analysis (vehicle control 1.00 ± 0.00; TGFβ2, 0.94 ± 0.22; TGFβ2 + GsMTx4, 1.11 ± 0.10; GsMTx4, 0.78 ± 0.23).
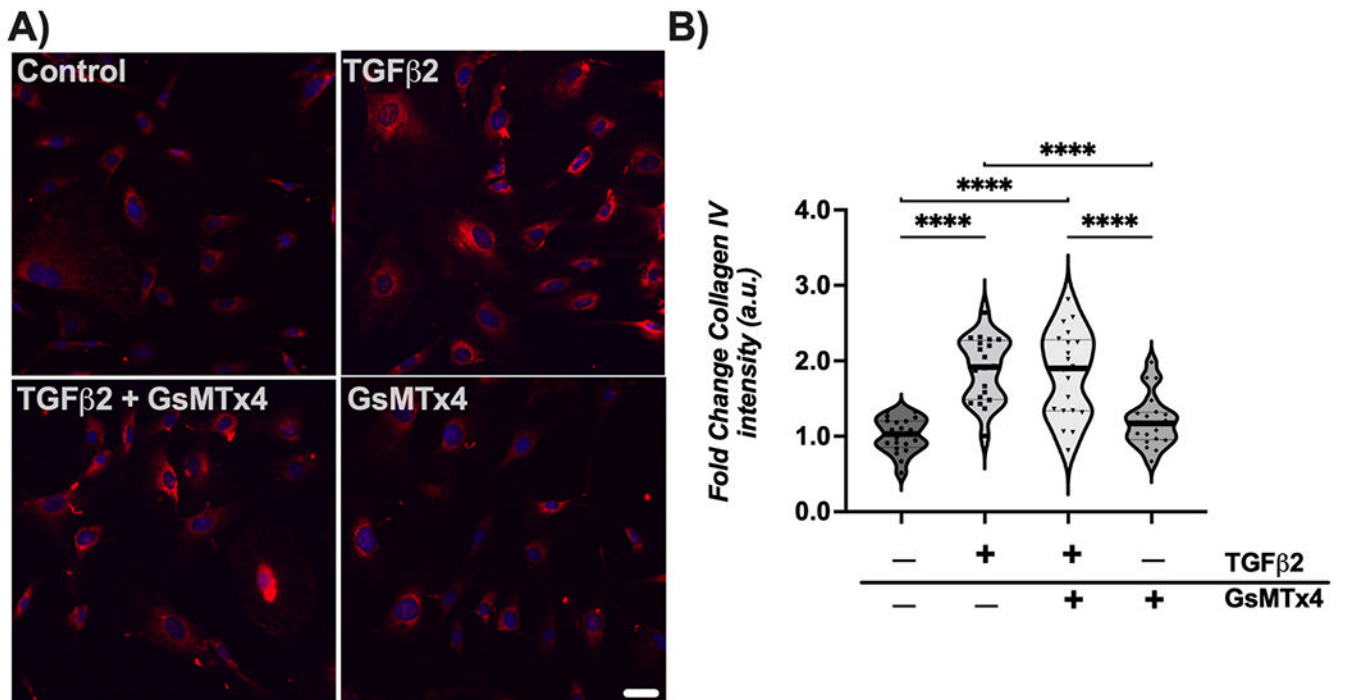
Fig. 5. Effect of mechanosensitive channel inhibition on TGFβ2-induced collagen IV immunoreactivity.

(A) Representative fluorescence images of collagen IV within ONH astrocytes following treatment for 48 h (collagen IV = red, DAPI = blue). Scale bar 50 μm. **(B)** Quantification of fold change in fluorescence intensity (mean ± SD, arbitrary units) after above treatments for 48 h (vehicle control, 1.01 ± 0.23; TGFβ2, 1.88 ± 0.43; TGFβ2 + GsMTx4, 1.82 ± 0.57; GsMTx4, 1.20 ± 0.34; ****$p < 0.0001$)